Taylor & Francis
Taylor & Francis Group

SEPARATION SCIENCE AND TECHNOLOGY

Separation Science and Technology

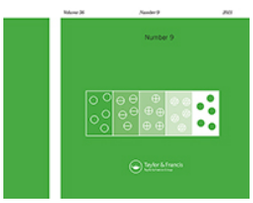

ISSN: (Print) (Online) Journal homepage: https://www.tandfonline.com/loi/lsst20

Rigorous rate-based model for CO_2 capture via monoethanolamine-based solutions: effect of kinetic models, mass transfer, and holdup correlations on prediction accuracy

Mahsa Amirkhosrow, José-Francisco Pérez-Calvo, Matteo Gazzani, Marco Mazzotti & Ebrahim Nemati Lay

To cite this article: Mahsa Amirkhosrow, José-Francisco Pérez-Calvo, Matteo Gazzani, Marco Mazzotti & Ebrahim Nemati Lay (2021) Rigorous rate-based model for CO_2 capture via monoethanolamine-based solutions: effect of kinetic models, mass transfer, and holdup correlations on prediction accuracy, Separation Science and Technology, 56:9, 1491-1509, DOI: 10.1080/01496395.2020.1784943

To link to this article: https://doi.org/10.1080/01496395.2020.1784943

SEPARATION SCIENCE AND TECHNOLOGY
2021, VOL. 56, NO. 9, 1491–1509
https://doi.org/10.1080/01496395.2020.1784943

Taylor & Francis
Taylor & Francis Group

Rigorous rate-based model for CO_2 capture via monoethanolamine-based solutions: effect of kinetic models, mass transfer, and holdup correlations on prediction accuracy

Mahsa Amirkhosrow[a,b], José-Francisco Pérez-Calvo[b], Matteo Gazzani[c], Marco Mazzotti[b], and Ebrahim Nemati Lay[a]

[a]Department of Chemical Engineering, Faculty of Engineering, University of Kashan, Kashan, Iran; [b]Institute of Energy and Process Engineering, ETH Zurich, Zurich, Switzerland; [c]Copernicus Institute of Sustainable Development, Utrecht University, Utrecht, The Netherlands

ABSTRACT

The existing rate-based modeling of monoethanolamine (MEA) solvent for CO_2 capturing has been improved using different kinetic models. Different models obtained from a combination of 15 kinetic models and 4 mass transfer correlations have been applied. The results show that the mass transfer correlation is instrumental for a reliable rate-based model. The resulting framework predicts the temperature and composition profiles at both liquid and gas phases with good accuracy. Overall, this allowed for improved prediction of (i) the CO_2 capture performance, (ii) the CO_2 partial pressure in output gas, and (iii) the temperature and CO_2 composition profiles in the liquid.

ARTICLE HISTORY
Received 14 March 2020
Accepted 15 June 2020

KEYWORDS
CO_2 capture; absorber; monoethanolamine; rate-based; kinetic model; mass transfer correlation

Introduction

The mitigation of CO_2 emissions is pivotal to prevent global warming. This requires the adoption of a variety of CO_2-neutral technologies. Among these, post-combustion CO_2 capture (PCC) from flue gas is a commercial technology that can be used to reduce CO_2 emissions from a variety of fossil fuel-derived flue gases.[1–6] A number of PCC technologies have been already demonstrated at pilot plant scale or higher, such as chemical absorption technologies using liquid solvents, adsorption processes using solid-phase sorbents or calcium looping technologies; other PCC technologies, although also studied extensively, are in an early stage of development, such as chemical looping, membrane-based, and ionic liquid capture technologies.[7,8] Chemical absorption using aqueous amine solutions is the benchmark PCC process due to its higher technology readiness level; while the exact recipe of commercial versions (i.e., MHI process, [9] Shell Cansolv'[10] and Aker solutions[11]) is mostly unknown, monoethanolamine (MEA) is regarded as the reference, well-known, solvent. Solvent-based capture technologies offer many advantages for CO_2 mitigation, yet it requires large-scale equipment to process the high volumes of flue gas, along with high energy consumption for solvent regeneration.[2,4,12-14] Choosing the proper solvent and the operating conditions of the PCC is essential for enhancing the performance; hence, a detailed assessment and analysis of this process is crucial for designing efficient PCC plants.[14,15] Development of accurate models for simulation of the behavior of PCC plants is a pivotal step aimed at the design, optimization, and scale up of CO_2 capture plants.[16]

Developing a precise and reliable model to predict the behavior of the absorption processes in carbon capture systems is key for the optimal design of such plants. Rate-based models have been proven to accurately describe packed columns, while also providing more information compared to equilibrium stage models, [17–19] especially with regards to the dynamic operation, [20] and the design and sizing. More specifically, rate-based models are not only able to describe the thermodynamics of highly non-ideal systems of multicomponent mixtures, such as those resulting of the reactive absorption of CO_2 with aqueous amine solutions. Furthermore, they are also capable of taking into account the mass and heat transfer limitations between the vapor and the liquid phase by coupling the diffusion of species and its coupling with the chemical reaction kinetics in the liquid phase.[21] However, developing a rate-based model demands a wide range of accurate input parameters to describe the physiochemical properties of both liquid and gas phases, kinetics, mass and heat transfer, and hydrodynamic of the process.[18]

CONTACT Ebrahim Nemati Lay enemati@kashanu.ac.ir Department of Chemical Engineering, Faculty of Engineering, University of Kashan, Kashan, Iran; Marco Mazzotti, marco.mazzotti@ipe.mavt.ethz.ch Institute of Process Engineering, ETH Zurich, Zurich 8092, Switzerland

In the MEA-based PCC process, CO_2 and MEA form a weak aqueous electrolyte solution that results in high non-ideal liquid phase.[2] This non-ideality needs to be reproduced by an accurate thermodynamic model when calculating the vapor-liquid equilibrium (VLE) of the system. The VLE data for gas solubility in aqueous solution of MEA are reported in literature for a wide range of MEA concentrations.[22–25] Based on these experimental data, different thermodynamic models are developed to describe this complex system. Accordingly, Wagner et al.[26] developed a model based on the extended Pitzer model [27,28] for electrolyte solutions; the Electrolyte Non Random Two Liquid (e-NRTL) method developed by Chen and Evans[29] is also commonly used to describe properties of such solutions.[14,24,30-32] The extended UNIQUAC model is another suitable thermodynamic framework for such systems.[22,33,34]

The reaction kinetics and the mass transfer of reactive species are two important, interconnected, factors that affect chemical absorption processes. In particular, the computation of the reaction rate between CO_2 and an aqueous solvent greatly impacts the simulation and analysis of the absorber.[35] Kinetically rate-controlled reactions in the MEA-CO_2-H_2O system have been widely studied and kinetic data are available in literature.[36–41] These allow to build kinetic models, which are instrumental for robust, reliable rate-based model.[18,42,43] Different theoretical approaches can describe the mass transfer at the gas-liquid interface.[44,45] The two film theory proposed by Lewis and Whitman in 1924[46] is often used for mass transfer modeling of CO_2 capture processes [47,48]; the penetration theory or surface renewal theory are also applied for mass transfer modeling.[42,49]

Developing a rate-based model for PCC processes requires a detailed study of numerous parameters. Previous research into rate-based modeling of MEA solvents is quite exhaustive[17,48,50-54]; however, few of these effective parameters are considered in these models. Especially: (i) there is no clear procedure on how to set up the numerical simulation of packed columns via rate-based models, e.g., in Aspen Plus, and (ii) there is no comprehensive comparison between the many rate-based models proposed and real pilot plant data. Accordingly, in this work we report a rigorous rate-based model of MEA-based CO_2 capture process for the absorption column; the model was developed in Aspen Plus (version 8.6) and was validated based on the CO_2 capture pilot plant tests at the Kaiserslautern University, [55] which has been used in several other works.[47,50,52,56] The model builds upon all experimental campaigns carried out by Notz et al., [55] and tests the different kinetic rate expressions available in literature. In this work, we discuss the main factors affecting the modeling framework: thermodynamics, axial discretization of the absorption column, discretization of the liquid film, mass transfer and interfacial area correlations, kinetic reaction equations, flow model, liquid holdup, and pressure drop. The fine-tuning of the rate-based model of the absorber was done by adjusting: (i) the vertical discretization, which is important for the accuracy of the model, [35,54,57] (ii) the liquid film discretization, which was done by optimizing the number of discretization points and discretization ratio, and (iii) the combination of kinetic models and mass transfer correlations. Ultimately, we not only provide an accurate rate-based model implemented in Aspen Plus, but also a clear procedure to implement new models for new solvents in general absorption process simulation environments. Due to the different temperature and CO_2 concentrations in the CO_2 absorber and in the CO_2 desorber, another rigorous rate-based model has been developed for the regeneration section of the capture process using aqueous MEA as solvent, [58] which also uses all the pilot plant experimental data reported by Notz et al. for the regeneration section.[55] Both rate-based models, i.e., for the absorber and for the desorber, have been developed to enable, when combined, a feasible and reliable optimization – in terms of energy and equipment size minimization – of CO_2 capture processes using aqueous MEA solutions as solvent.

Rate-based modeling methods

The rate-based approach provides a detailed description of reactive absorption columns. This approach demands more computational time compared to the equilibrium-based approach due to the larger number of equations to be solved. While the rate-based framework of Aspen Plus, version 8.6, which makes use of the two-film theory, offers an efficient implementation approach, the off-the-shelf availability might lead to partial implementation of the different setting parameters. Hereafter, we summarize the key features of the proposed modeling framework.

Thermodynamic model

The Soave-Redlich-Kwong Equation of State (SRK EOS) for the vapor phase

Due to the low operating pressure of an absorber, the vapor phase has little deviation from ideality; this non-ideality is negligible and an equation of state can be used to determine the vapor phase properties.[59] Accordingly, the SRK EOS[60] was used to determine

the fugacity coefficient of vapor phase in this study. This equation has been used by several groups and has successfully predicted the gas phase properties along the CO_2 absorber.[32,47,56,59] Parameters of SRK EOS were obtained from SRK-ASPEN databank.[50] The correlations are presented in equations S-6 to S-10 in the Supporting Information.

The e-NRTL approach for the liquid phase

In the present work, the e-NRTL method, which is widely applied for thermodynamic modeling of PCC processes using amine solvents, [14,24,30-32] was used to compute the liquid phase properties, including activity coefficients, Gibb's free energy, enthalpy, and entropy. This method accurately takes into account the interactions between molecule-molecule, ion-ion, and molecule-ion pairs; hence, based on these binary pair parameters, this model can determine the liquid speciation for both ionic and molecular species in aqueous and mixed solvent electrolyte systems. A large number of parameters are involved in the VLE calculation of this model. Aspen Plus developed a rigorous thermodynamic model using the e-NRTL framework based on several experimental VLE data.[50] Henry's law was used to describe the thermodynamic equilibrium at the gas-liquid interface. The correlations are presented in equations S-1 to S-5 in the Supporting Information.

Equilibrium reactions

The absorption of CO_2 into an aqueous solution of MEA is controlled by a series of chemical reactions. Therefore, the chemical equilibrium reactions (equations (1)-(5)) should be considered for reactive absorption of CO_2. In these reactions, CO_2, MEA, and all ionic species are considered as solutes and water is treated as the solvent. The chemistry of an electrolyte solution is modeled with the chemistry model of Aspen Plus based on the following equations[61]:

$$2H_2O \rightleftarrows H_3O^+ + OH^- \quad (1)$$

$$CO_2 + 2H_2O \rightleftarrows H_3O^+ + HCO_3^- \quad (2)$$

$$HCO_3^- + H_2O \rightleftarrows H_3O^+ + CO_3^{2-} \quad (3)$$

$$MEAH^+ + H_2O \rightleftarrows H_3O^+ + MEA \quad (4)$$

$$MEACOO^- + H_2O \rightleftarrows MEA + HCO_3^- \quad (5)$$

The equilibrium constants of reactions (1)–(5) were calculated by the following temperature-dependent correlation in Aspen Plus chemistry model:

$$\ln(K_{eq}) = \frac{A}{T} + B\ln T + C \quad (6)$$

where K_{eq} is the reaction equilibrium constant, A, B, and C are parameters of the equilibrium constants, and T is the absolute temperature (K). Table 1 shows the equilibrium constants that were used in this study.

Transport property models

The liquid molar volume and, hence, the liquid density, was estimated by the Clark model with the quadratic mixing rule for solvents. For estimation of the liquid viscosity, the Jones-Dole electrolyte correction model was applied in Aspen Plus. The Onsager-Samaras model was used for liquid surface tension estimation and the thermal conductivity was calculated using the Riedel electrolyte correction model. The binary diffusivity was calculated by Nernst-Hartley model in Aspen Plus. All the parameters of these correlations and also the aqueous phase Gibbs free energy, heat of formation at infinite dilution and 25°C, and heat capacity at infinite dilution were obtained from Aspen Plus data bank. The applied transport property models have been validated with experimental data by Aspen Tech.[50]

Kinetically-controlled reactions

The reactions that only involve the transfer of a proton can be assumed to reach equilibrium instantaneously, i.e., reactions (1), (2), and (4), while the reaction of CO_2 with MEA and with the hydroxide ion are kinetically controlled and require a reliable computation of the reaction rate.

The reaction mechanism of carbon dioxide and MEA is thoroughly described in literature.[36–39] In the overall reaction, equation (7), two MEA molecules react with one CO_2 molecule to form the carbamate ion and protonated MEA, which is a linear combination of reactions given by equation (2), equation (4) and equation (5).

$$2MEA + CO_2 \rightleftarrows MEACOO^- + MEAH^+ \quad (7)$$

Ultimately, two mechanisms have been used to explain the reaction pathway: one based on the formation of a zwitterion and its following deprotonation, [64,65] and

Table 1. Equilibrium constants parameters.

Reaction	A	B	C	Temperature (K)	Reference
1	−13445.9	−22.4773	140.932	273–498	[62]
2	−12092.1	−36.7816	235.482	273–498	[62]
3	−12431.7	−35.4819	220.067	273.498	[62]
4	−3090.83	0.0	6.69425	298–413	[63]
5	−5851.11	0.0	−3.3636	298–413	[63]

one based on a termolecular mechanism.[66] Notably, the zwitterion mechanism can be reduced under certain assumptions[67] to either a simple second-order kinetics, or to the termolecular mechanism, with the following expressions for the reaction rate, respectively:

$$r_{CO_2} = -k_2[MEA][CO_2] \quad (8)$$

$$r_{CO_2} = -[MEA][CO_2] \cdot (k_{MEA}[MEA] + k_{H_2O}[H_2O]) \quad (9)$$

Various kinetic constants are available in the literature to calculate the rate of reaction (7) by means of equations (8) and (9). However, only some of them considered the dependency of the reaction rate constant on temperature and reported an equation based on a specific temperature range. Tables 2 and 3 provide the reported reaction rate constants available in literature in power law form. These kinetic constants were obtained independently using different experimental methods in different ranges of temperature, MEA concentration, and CO_2 loading, which therefore led to different values. In this study, all reaction kinetics reported in Tables 2 and 3 were implemented in Aspen Plus, aiming at identifying those were able to better reproduce the experimental results of Notz et al.[55]

On the other hand, the reaction between CO_2 and the hydroxide ion takes place in parallel to that of CO_2 with MEA, which is a linear combination of the reactions given by equation (1) and equation (2):

$$CO_2 + OH^- \rightleftharpoons HCO_3^- \quad (10)$$

Several authors have measured this reaction rate, [75–77] notably leading to the identification of similar reaction rate constants when the ionic strength of the solution is considered.[77] Nevertheless, the absorption of CO_2 into aqueous amine solutions is dominated by the reaction of CO_2 with the amine if typical amine concentrations of PCC processes are used.[78] Consequently, the impact of the reaction rate constant of the reaction between CO_2 and the hydroxide ion on the accuracy of the model has been neglected and its value has been retrieved from the work of Pinsent et al.[79]

Both forward and reverse reactions were considered, so to accurately predict conditions at high CO_2 loadings. These were calculated using the forward kinetic constants and the equilibrium constants (see section 2–1 in the Supporting Information).

Mass transfer, heat transfer and hydrodynamic properties

Reliable mass transfer and hydrodynamic correlations are very important components of the model, as they define the column hydraulics, liquid holdup, and pressure drop. Moreover, they contribute to the multicomponent Maxwell-Stefan diffusion equation used to calculate the gas and liquid phase mass transfer rates in an Aspen Plus. Previous works revealed (i) the impact of mass transfer correlations and effective interfacial area on the accuracy of a rate-based model, [17,80,81] as well as (ii) the role of hydrodynamic performance of the column on the design and scale up of this process.[47,56,82,83]

Table 2. The literature data of second-order rate constants.

Temperature (K)	[MEA] (kmol/m^3)	[CO_2] (kmol/m^3)	k_2 (m^3/kmol s)	Experimental method	Reference
278–308	0.152–0.177	0.0039–0.0064	9.770×10^{10} exp (−4955.0/T)	Rapid mixing	Hikita et al.[38]
278–303	0.0091–0.06	0.00096–0.0032	1.230×10^{11} exp (−5078.0/T)	Stopped flow	Penny and Ritter[68]
278–298	0.00–0.45	0.013–1.50	8.510×10^{11} exp (−5617.0/T)	Stopped flow	Alper[37]
303–313	0.10–0.50	0.00	3.014×10^{11}exp (−5376.2/T)	Wetted wall column	Horng and Li[39]
303–334	0.63	0.00	4.500×10^{11} exp (−5405.0/T)	Stirred cell reactor	Kucka et al.[41]
298–313	0.005–0.035	0.00	8.360×10^{11} exp (−5613.0/T)	Stopped flow	Ali[69]
278–313	0.00–4.80	0.00096–1.5	4.400×10^{11} exp (−5400.0/T)	-	Versteeg et al.[70]
288–318	0.001–0.016	0.003–0.006	5.800×10^{10} exp (−4872.0/T)	Stopped flow	Conway et al.[71]
298–323	0.50–12.00	0.00	4.140×10^{11} exp (−5399.0/T)	Stirred cell reactor	Ying and Eimer[72]
298–343	1.00	0.00–0.40	8.870×10^{8} exp (−3458.0/T)	Wwc&SD[a]	Luo et al.[6] – Model a
298–343	5.00	0.00–0.40	4.396×10^{9} exp (−3693.0/T)	Wwc&SD	Luo et al.[6] – Model b

[a]: Wetted wall column and string of disc

Table 3. The literature data of termolecular rate constants.

Temperature (K)	[MEA] (kmol/m^3)	[CO_2] (kmol/m^3)	k_{MEA} (m^6/kmol^2 s)	k_{H2O} (m^6/kmol^2 s)	Experimental method	Reference
293–333	0.19–6.00	0.10–0.49	4.610×10^{9} exp (−4412/T)	4.550×10^{6} exp (−3287/T)	Laminar jet	Aboudheir et al.[36]
298–343	0.50–5.00	0.00–0.40	8.070×10^{9} exp (−4503/T)	3.510×10^{6} exp (−3055/T)	Wwc&SD[a]	Luo et al.[73]
298–343	1.00&5.00	0.00–0.40	2.003×10^{10} exp (−4742/T)	4.147×10^{6} exp (−3110/T)	Wwc & SD	Luo et al.[6] – Model c
293–343	0.00–5.00	0.00–0.50	3.173×10^{9} exp (−4936.6/T)	1.088×10^{8} exp (−3900/T)	–	Putta et al.[74]

[a]: Wetted wall column and string of disc

Mass transfer coefficients and specific interfacial area

Various mass transfer correlations are available in the literature for packed columns with random and structured packings.[84–89] The Aspen Plus rate-based framework provides four empirical correlations for the estimation of mass transfer coefficients and vapor-liquid interfacial area.[85,87-89] The Aspen Plus rate-based model provides all parameters that are needed for implementing these correlations except for two parameters of Billet and Schultes[85] mass transfer correlation, i.e., C_L and C_V, which are constants included in the liquid and vapor mass transfer coefficients, respectively. However, no data are available for such constants of Mellapak 250.Y^{TM} structured packing used in the pilot plant tests considered in this study. Therefore, the C_L and C_V of Mellapak 250.Y^{TM} were estimated by adopting the packing constants obtained for Ralu pak (250 YC) by Billet and Schultes[85] (see Table 4). Both of these packings are structured packing of corrugated metal sheet and despite the difference in corrugation angle and their vendors, they have the same surface area (see Table 4) and void fraction[90]; that makes it possible to use the constants of Ralu pak (250 YC) as estimated values for the correlation constants of Mellapak 250.Y^{TM}.

The Chilton-Colburn analogy between heat and mass transfer was used in this study for estimating the heat transfer coefficients.

Liquid holdup and pressure drop

For an absorber consisting of a packed column, the hydrodynamic performance is mainly represented by pressure drop and liquid holdup. The liquid holdup enables the determination of the pressure drop and fluid effective velocity and affects the mass transfer in the packed columns. The gas holdup can usually be ignored due to the low gas-phase density. A number of empirical correlations for determination of liquid holdup are available in the literature.[91–95] The Aspen Plus rate-based framework, provides three correlations for holdup estimation.[85,89,95] In this work, we investigate the effect of different liquid holdup correlations on the model predictions. In terms of pressure drop, our model relies on the values provided by the pilot tests, which also significantly reduces the computational time of the model. This parameter was fixed to 1.74 mbar/m.[55]

Table 4. Characteristics of the structured packings[90] and the constants of C_L and C_V in Billet and Schultes mass transfer correlation.[85].

	Packing type	
Characteristic	Ralu pak	Mellapak 250.Y^{TM}
Material	Sheet metal	Sheet metal
Nominal size (mm)	250 YC	250 Y
Degree corrugation angle	60 Degree (with the horizontal)	45 Degree
Surface area (m^2/m^3)	250	250
% Void	95	95
Packing Factor (m^{-1})	-	66
Vendor	Rasching AG Ludwigshafen, Germany	Sulzer Chemtech Tulsa, Oklahoma; Winterthur, Switzerland
C_L (-)	1.334	n.a.
C_V (-)	0.385	n.a.

Numerical options

Flow model

The flow model determines how the bulk properties are calculated along the column and is therefore key for proper mass and energy flux, and reaction rate computations. Aspen Plus offers four different flow models including Mixed, CounterCurrent, V-Plug, and L-Plug. However, the flow model has a minor effect on the overall CO_2 absorption performance whenever the axial discretization of the column is fine enough.[5,54] We therefore did not investigate the effect of different flow models and chose the V-Plug model, which is recommended by other authors in literature.[15,47,80,87] Based on the V-Plug flow model, the outlet conditions are used for the bulk of liquid and average conditions are used for the vapor bulk; the average pressure is used.

Axial discretization

The axial discretization of the packed column divides it into a number of control volumes; each control volume consists of liquid and vapor phases, divided between the bulk and the film, in which mass and energy balances are solved.[53] The goal of the axial discretization analysis is to find minimum number of segments that makes the numerical error of the model acceptable. A finer grid (more number of segments) decreases the numerical error of the model, but increases the computational time. The error is computed considering as reference a case with an extremely fine axial discretization. Thereafter, due to the high computational time of the reference case, a lower segments number that led to an acceptable numerical error with respect to the base case was selected.

Film discretization

The discretization of the liquid film significantly affects the reliability of a rate-based model as it controls the mass transfer resistances and the kinetically controlled chemical reactions in the liquid film layer that enhances the CO_2 absorption rate.[54] Conversely, the discretization of the vapor film is not required as no significant

chemical reaction takes place in the vapor phase. In this work, the key parameters of the liquid film discretization were investigated, which include film discretization ratio and number of discretization points. Aspen Plus provides two film discretization options: arithmetic and geometric, both with parameters to be adjusted for accurate modeling. The geometric discretization of the liquid film is expected to mimic the real profiles within the film with less segments compared to the arithmetic discretization, as it is able to better describe steep CO_2 concentration decays next to the interphase, which are typical of reactive absorption processes. Therefore, in this study, we use a computationally intensive arithmetic approach to simulate the reference case, which is then used to tune the experimental simulations with the geometric approach that should make the model faster for the same required accuracy. The arithmetic discretization requires the definition of a discretization increment, which control the thickness of adjacent film regions. This parameter was set to 1 in order to create segments with equal thickness, while the number of discretization points (NDP) was set at the maximum number possible in Aspen Plus, i.e., 50. This setting features high convergence time but discretizes the film well. Thereafter, 60 trial cases applying the geometric discretization with 5 and 12 different NDP and film discretization ratio (FDR), respectively, were simulated (FDR is the thickness of each film region over thickness of the next region).

It should be noted that the other numerical parameters of the rate-based model which are not mentioned were set to the default values provided in Aspen Plus.

Pilot plant tests for model validation

Experimental data for model comparison and validation were retrieved from a comprehensive pilot plant campaign carried out at Kaiserslautern University.[55] Fig. 1a shows a schematic of the absorption column based on experiment 1 in Notz et al. The column comprises a washing part and a CO_2 absorption part, with one and five packing sections, respectively, equipped with Mellapak 250.Y^{TM} structured packing. The specifications of the absorption column are summarized in Table 5. Flue gas was fed into the absorber at the bottom of the lowest packing section and lean solvent at the top of the fifth packing section (defining the CO_2 capture section). The water-wash section at the top of the absorber above the lean solvent feed reduces amine losses. The water was recycled (stream 14) from the liquid collector and cooled to the design temperature prior to feeding into the top of the section. Fresh water was continuously mixed with the recycled water to prevent amine accumulation (for more details refer to[55]). Figure 1b shows the absorption column simulated in Aspen Plus, version 8.6, in this study. The water-wash section of the absorber was split in the simulation sheet

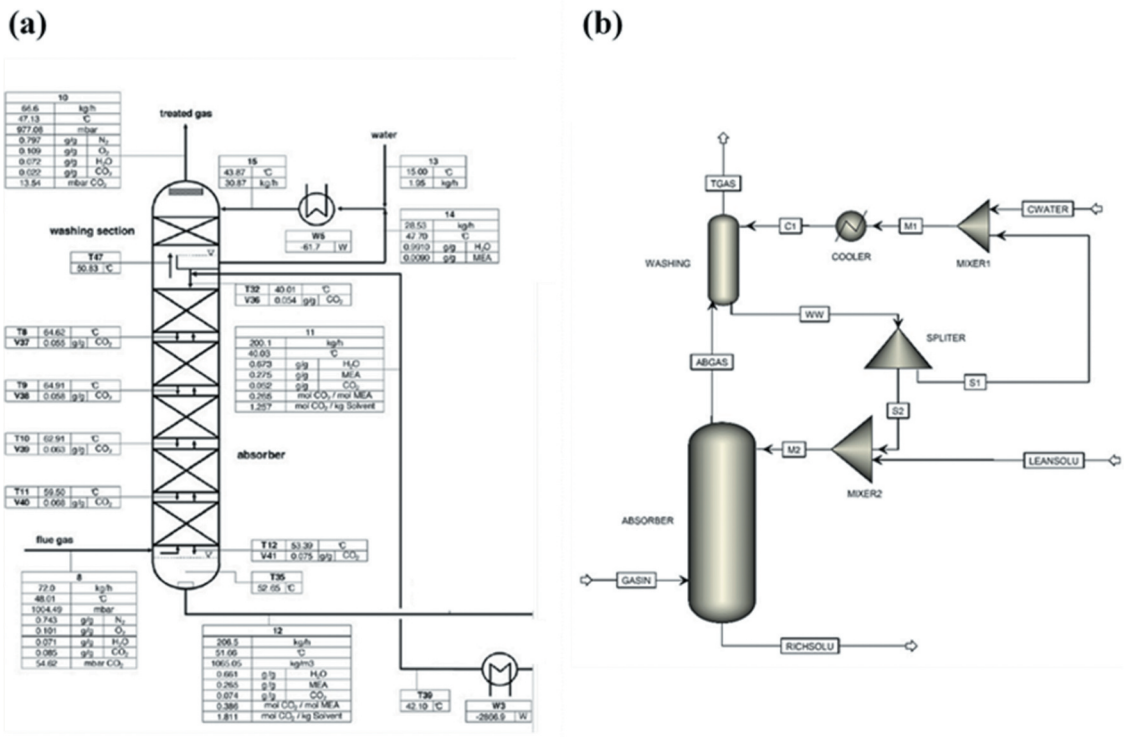

Figure 1. (a) The absorption column in experimental work by Notz et al.[55] and (b) the simulated absorption column in this work.

Table 5. Specification of the CO_2 absorber of the pilot plant according to selected runs.[55].

Column Specifications	
Column internals	Structured packing, Sulzer Mellapak 250.Y^{TM}
Height of packing in Absorber (m)	4.20
Height of packing in Washing section (m)	0.42
Packing material	Stainless steel
Diameter of columns, absorber and washing section (m)	0.125
Pressure at the Absorber (bar)	1.013
Pressure drop (mbar/m)	1.74

to reduce the convergence time of the process; a splitter was used to recycle the washing water.

Notz et al. have reported 47 runs with differing operating conditions such as CO_2 partial pressure in the flue gas, liquid and gas temperatures, liquid and gas flowrates and CO_2 lean loading, which have all been used here to validate the model. In our work, we use four pilot plant experiments to compare models and to identify the best combination of mass transfer and kinetic model. The four experiments were selected (i) to be representative of both natural gas and coal power plants, and (ii) to have a remarkable difference in the CO_2 partial pressure in the flue gas. Accordingly, experiments 1 and 2 in Notz et al. replicate the conditions of a gas-fired power plant and a coal-fired power plant, while experiments 6 and 3 have the highest and lowest CO_2 partial pressure in flue gas, respectively. For the sake of brevity, the results corresponding to experiment 1 (EXP1) and experiment 2 (EXP2) are shown in this main text, and experiment 3 (EXP3) and experiment 6 (EXP6) are reported in the Supporting Information. Following the identification of the most performing combination, the rate-based model is assessed using all 47 experiments reported by Notz et al.

Table 6 provides the operating conditions related to the selected runs of Notz et al. pilot plant, [55] including the flue gas and lean solvent conditions, as well as the heat loss of the absorber reported in each experiment. Notz et al. reported the precision of their devices in main flow measurement in range of 0.2–1% and the accuracy of temperature and pressure measurement equal to 0.1° C and 1–2 mbar, respectively.

The following equations were used to calculate the CO_2 loading of the CO_2-rich stream, CO_2 rich loading ($molCO_2/molMEA$), the CO_2 capture efficiency, CO_2 captured (%), and the corresponding errors with respect to either experimental data or reference simulations:

$$CO_2 captured = \frac{\left(_{CO_2,in} - _{CO_2,out}\right)}{_{CO_2,in}} \times 100 \tag{11}$$

$$CO_2 \text{ rich loading} = \frac{m/CO_2}{m/MEA} \tag{12}$$

$$\text{Absolute Relative Deviation(ARD)\%} = \frac{|\theta_E - \theta_m|}{\theta_E} \times 100 \tag{13}$$

$$\text{Average Absolute Relative Deviation(AARD)\%} = \left[\frac{\sum_{i=1}^{N}\left(\frac{|\theta_{base_i} - \theta_i|}{\theta_{base_i}}\right)}{N}\right] \times 100 \tag{14}$$

$$\text{Root Mean Square Deviations(RMSD)} = \sqrt{\frac{\sum_{j=1}^{M}\left(\theta_j - \theta_{base_j}\right)^2}{M}} \tag{15}$$

where $_{CO_2,in}$ and $_{CO_2,out}$ are the inlet and the outlet mass flow rates of CO_2 ($kg{\cdot}hr^{-1}$) to the absorption column, respectively, m/CO_2 and m/MEA are the apparent molar flow rates of CO_2 ($mol{\cdot}hr^{-1}$) and MEA in the CO_2-rich solvent stream, respectively. θ is the value of a process variable: θ_E is the experimental value, θ_m is the value

Table 6. Operating conditions of selected runs[55] for model tuning.

	EXP1		EXP2		EXP3		EXP6	
Variables	Flue gas	Lean solvent	Flue gas	Lean solvent	Flue gas	Lean solvent	Flue gas	Lean solvent
Temperature (°C)	48.01	40.03	48.15	40.18	40.61	39.81	47.76	40.05
Pressure (mbar)	1004.49	1004.49	1009.66	1009.66	1007.45	1007.45	1011.29	1011.29
Total flow rate (kg/h)	72.0	200.1	72.4	200.0	72.1	200.0	72.1	200.0
CO_2 (mass fraction)	0.085	0.052	0.165	0.063	0.055	0.048	0.198	0.065
H_2O (mass fraction)	0.071	0.673	0.069	0.653	0.048	0.665	0.067	0.649
MEA (mass fraction)	0.000	0.275	0.000	0.284	0.000	0.287	0.000	0.286
O_2 (mass fraction)	0.101	0.000	0.094	0.000	0.148	0.000	0.092	0.000
N_2 (mass fraction)	0.743	0.000	0.672	0.000	0.749	0.000	0.643	0.000
Absorber Heat loss (W)	−81.7		−193.0		−84.8		−349.1	

predicted by the model, i is the segment number along the axial discretization of the column (here, i = 1, 2, …, N = 50), θ_i is the estimated value at segment i, $\theta_{base,i}$ is the predicted value by the base case model at segment i, j is the segment number within the discretized liquid film (here, j = 1, 2, …, M = 12), θ_j is the estimated values at segment j, and $\theta_{base,j}$ is the predicted value by the base case model at segment j.

Results and discussion

In the following, we first report the results for the numerical calibration of the rate-based model, and thereafter investigate the different building blocks of the rate-based models.

Tuning the discretization: column and liquid film

The calibration of the numerical options for modeling the system was carried out using (i) the kinetic model proposed by Aboudheir et al., [36] (ii) the mass transfer correlations by Bravo et al., [88] and (iii) the liquid holdup correlation by Bravo et al.[89]

Axial discretization of the column

As previously mentioned, the optimal number of finite volumes of the column was identified by comparing the model results against a base case with extremely fine grid. Table 7 presents the features of the different cases tested regarding the CO_2 capture section and the water-wash section of the absorber. The overall height of the packing is fixed as in Notz et al. (CO_2 capture section = 4.2 m and water-wash section = 0.42 m).[55]

The prediction of the CO_2 mass fraction in the gas stream exiting the top of the water-wash section for different axial discretization of the column is shown in Fig. 2. It can be noted that the prediction of the model is a strong function of the axial discretization of the column for a coarse discretization mode, but it tends toward an asymptotic value with a finer discretization. There exists a threshold for the axial discretization of the column for which a finer discretization increases the computational demands of the model without affecting significantly the results predicted. Ultimately, the minimum number of segments was identified by comparing the root mean square deviations (RMSD) of the temperature and CO_2 mass fraction in the liquid and gas along the packed column (Table 8).

It can be noted that the RMSD is small for the CO_2 concentration in the liquid and in the gas, while it is remarkable for the temperature profiles in both the liquid and gas. However, for a discretization with less than 0.1 m per segment (case 4 in Table 7, highlighted values in Table 8), all RMSD are below the unit. Accordingly, 55 segments (50 segments in the absorber section, 5 in the washing section) were chosen as optimal axial discretization number, i.e., 0.0840 m per axial segment.

Table 7. Base case and studied cases varying the height per segment for the axial discretization of the column.

	Number of segments		height per
Case ID	CO_2 capture section	Water-wash section	segment (m)
1	20	2	0.2100
2	30	3	0.1400
3	40	4	0.1050
4	50	5	0.0840
5	60	6	0.0700
6	70	7	0.0600
7	80	8	0.0525
8	90	9	0.0467
9	100	10	0.0420
10	200	20	0.0210
base case	**250**	**25**	**0.0168**

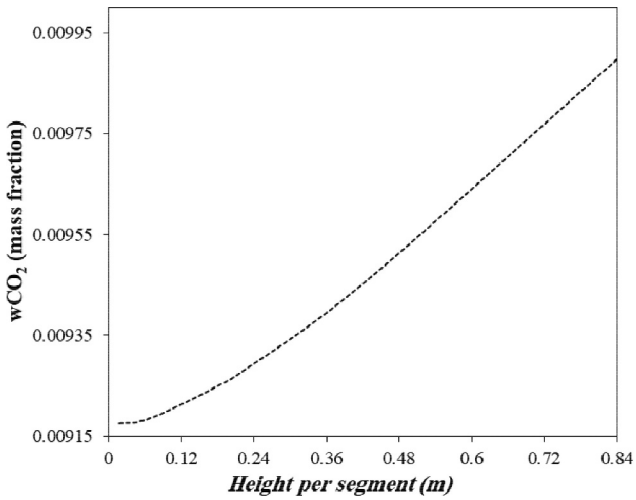

Figure 2. CO_2 mass fraction as a function of axial discretization in the gas phase at the top of the absorber.

Table 8. The RMSD of 10 cases with respect to the base case.

	Root Mean Square Deviation			
Case ID	Temperature (°C) (liquid)	Temperature (°C) (gas)	CO_2 mass fraction (g/g) (liquid)	CO_2 mass fraction (g/g) (gas)
1	2.00	2.45	3.93E-04	0.0032
2	1.32	1.59	2.68E-04	0.0021
3	0.96	1.14	2.01E-04	0.0015
4	0.74	0.87	1.63E-04	0.0012
5	0.59	0.69	1.33E-04	0.0009
6	0.48	0.56	1.13E-04	0.0008
7	0.40	0.47	9.67E-05	0.0006
8	0.34	0.39	8.76E-05	0.0005
9	0.29	0.33	7.57E-05	0.0004
10	0.05	0.06	2.19E-05	7.46E-05

Discretization of the liquid film

As mentioned, the base case was set by using the arithmetic discretization with a discretization increment of 1

and 50 NDP. The comparative evaluation was carried out by using the AARD% considering the CO_2 partial pressure along the absorber for four selected experiments (EXP1, EXP2, EXP3, and EXP6). Figure 3 reports the obtained results for EXP1, while the rest are reported in Figure S-4 in the Supporting Information.

As shown in Fig. 3, the curves feature similar AARD% profiles as a function of FDR and NDP; these curves have a minimum AARD% for FDR of 1.5–5. On the other hand, increasing NDP decreases the AARD% for a fixed FDR, with significant gain for low FDR, and limited effects for FDR larger than five. Lower FDR minimizes the AARD% when increasing the NDP, obtaining the optimum FDR of 1.5 for NDP equal to 6. Table 9 reports the corresponding values of AARD%. It is found that: (i) for NDP larger than 5, small changes in AARD% were obtained; and (ii) the suitable range of FDR values that minimizes the AARD% is broadened for larger NDP, although the optimum FDR of 1.5 is always obtained for NDP above 5. Therefore, the combination NDP = 6 and FDR = 1.5 provides a low enough AARD% value (highlighted value in Table 9) while limiting the computational time of the rate-based simulations. Further comparison of the base case and the optimized one in terms of CO_2 mass fraction and temperature profiles at interface of two phases along the column are presented in Figure S-5 of the Supporting Information.

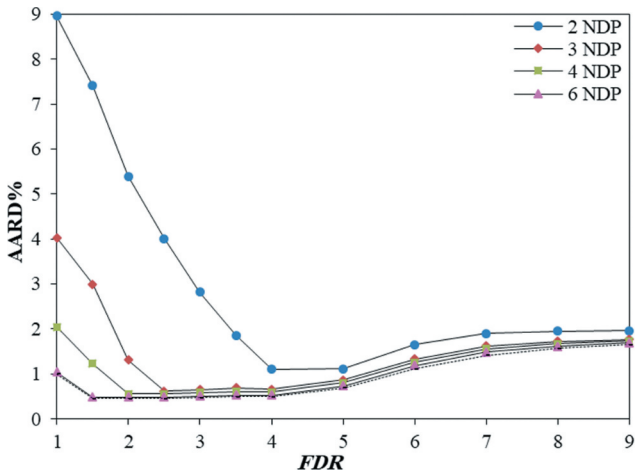

Figure 3. The AARD% of trial cases with respect to the base case.

Rate-based model screening and validation

Mass transfer coefficient and effective interfacial area correlations and kinetic model

The prediction capabilities of the rate-based model were assessed for all combinations of: (i) four mass transfer coefficients and effective interfacial area correlations available in Aspen Plus, version 8.6, for the Mellapak 250.Y^{TM} structured packing, and (ii) the kinetic models presented in Tables 2 and 3. The liquid holdup correlation proposed by Bravo et al.[89] was used in all cases. Figure 4 shows the liquid temperature profile predicted by each rate-based model along with the experimental data for EXP1. It is worth underlining that the temperature at 4.2 m represents stream M2 after the mixer in Fig. 1b; accordingly, the temperature profile between h = 4.2–4.62 m corresponds to the water-wash section, where no experimental data are available except for the temperature of the liquid stream entering at the top of the column (stream 15 in Fig. 1a). As shown in Fig. 4, the lowest liquid temperature occurs at the top of the column where the lean amine and the outlet of the water-wash section are mixed; as the solvent flows down through the column, the exothermic reaction between CO_2 and MEA increases the temperature. This leads to a temperature maximum within the column. The shape and location of the maximum is related to the flow rate of liquid and flue gas, to the solvent composition, to the heat of reaction, and to the CO_2 absorption rate along the absorption column.[96]

Clearly, all rate-based models feature similar trends, which are in line with the experimental data, except those using the Bravo et al. correlation from 1992, which underestimates the effective interfacial area[89] (Fig. 4b). Moreover, the models using the mass transfer correlations from Billet and Schultes[85] (Fig. 4c) show

Table 9. The AARD% of trial cases with different NDP and FDR with respect to the base case, considering the CO_2 partial pressure along the absorber for the computation of the AARD%, at the operating conditions of EXP1.

	AARD%							
	2	3	4	5	6	7	8	9
1	8.96209	4.02896	2.04546	1.24505	1.04185	1.01351	1.00671	0.99989
1.5	7.41210	3.00015	1.23149	0.5269	0.48506	0.48618	0.45112	0.4510
2	5.39967	1.30764	0.55309	0.51925	0.48645	0.48669	0.45121	0.45117
2.5	4.01304	0.61699	0.55484	0.52110	0.48708	0.48693	0.45128	0.45118
3	2.82181	0.65236	0.58293	0.54389	0.50832	0.50766	0.47185	0.47177
3.5	1.86326	0.68807	0.60536	0.56413	0.52829	0.52752	0.49180	0.49173
4	1.10849	0.6645	0.60249	0.56494	0.53013	0.52976	0.60882	0.49408
5	1.11047	0.86182	0.80099	0.7638	0.72919	0.72897	0.65128	0.69328
6	1.65418	1.33319	1.26324	1.22529	1.19069	1.1905	1.05334	1.11654

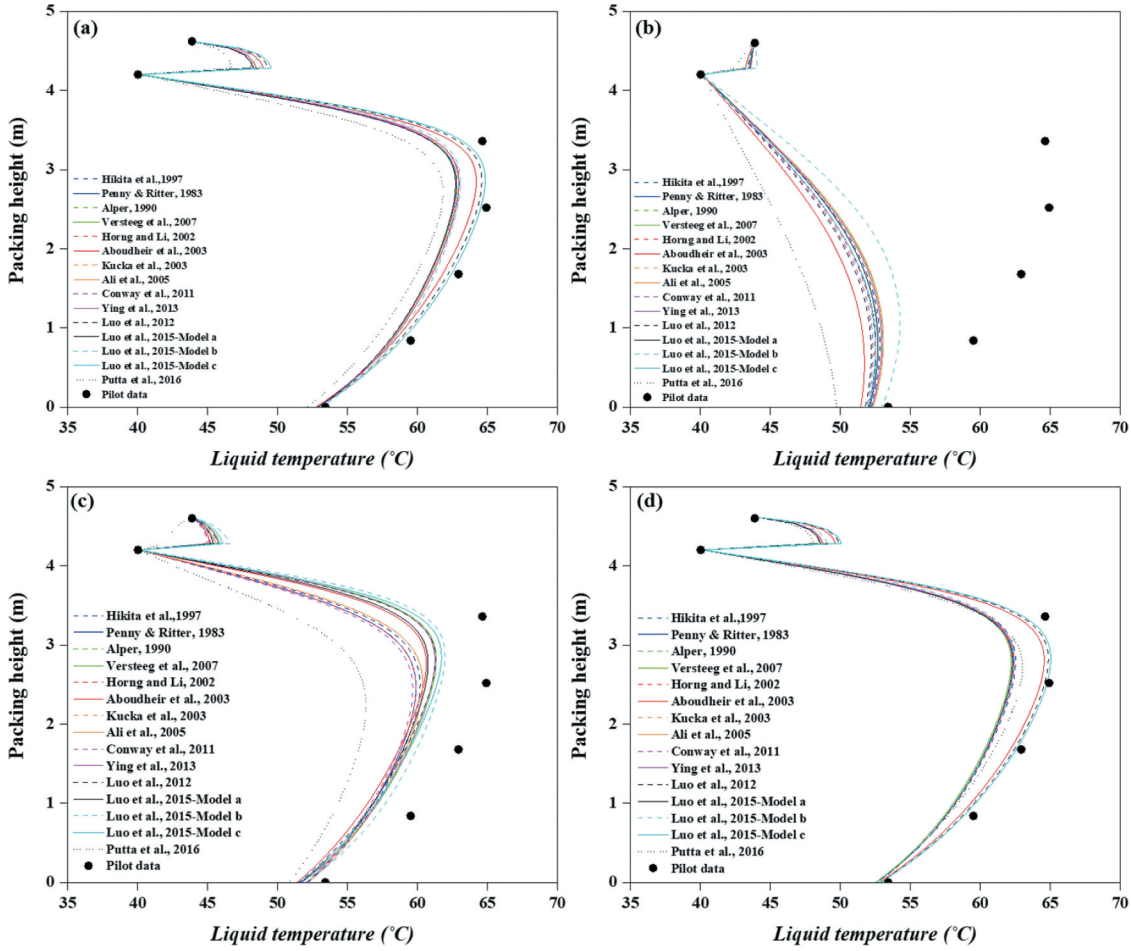

Figure 4. Liquid temperature profiles reported by Notz et al.[55] for their pilot plant test identified as EXP1 in Table 6, and predicted results by rate-based models using different kinetic models (reported in Table 2 and Table 3) and mass transfer correlations: (a) L. Bravo et al.,[88] (b) L. Bravo et al.,[89] (c) Billet and Schultes,[85] and (d) Hanley and Chen.[87].

higher deviations from the pilot data compared to the two other mass transfer correlations. This deviation likely arises from the correlation constants being based on a different type of structured packing (see section 2.3.1.); although the estimated constants of Mellapak 250.Y^{TM} were based on a packing with the same surface area, they were from different vendors and have different geometries (different degree of corrugation). Such differences may lead to inaccurate results of the models using Billet and Schultes[85] mass transfer correlation. The mass transfer correlation proposed by Hanley and Chen[87] (Fig. 4d) performs similar to Bravo et al. correlation from 1985[88] (Fig. 4a), with slightly higher temperature predictions along the absorption column.

When looking at the different kinetic models tested, we note that, in general, the kinetic models assuming termolecular mechanism are more accurate than those using second-order models. The key reason behind this result is that most of the second-order rate constants presented in Table 2 were obtained using aqueous solutions containing very low MEA concentration, where second-order kinetics seems to describe properly the reaction mechanism of CO_2 with MEA. On the other hand, the kinetic models based on a termolecular mechanism (Table 3) were selected when a wide range of MEA concentration had been used for the modeling of kinetics of the aforementioned reaction, similar conditions to those used in the pilot plant tests. Finally, we believe that the different results obtained with Putta's kinetic model[74] are because of the different thermodynamic model used for the parameter estimation (although the kinetics of the reaction of CO_2 with MEA in Putta are for a wide range of MEA concentrations and based on the termolecular mechanism).

Figure 5 illustrates the prediction of the CO_2 partial pressure along the column for the different models and mass transfer correlations for EXP1 (as for temperature in Fig. 4). As expected, the results are similar to what obtained for the liquid temperature profile: Bravo-1992[89] and Billet[85] fail to match the experimental

data, and the kinetic models based on a termolecular mechanism outperform those using a second-order reaction mechanism. In fact, Aboudheir et al., [36] Luo et al.-2012, [73] and Luo et al.-2015-Model c[6] provide the most accurate predictions, in all cases describing the reaction of MEA with CO_2 by means of the termolecular mechanism. The predicted mass fraction of CO_2 and the values of average absolute deviation from pilot data are reported in Figure S-6 and Table S-2 of the Supporting Information, respectively.

For the sake of conciseness and clarity, only the most promising combinations of mass transfer and interfacial area correlations and kinetic models were selected for further performance analysis and comparison. This resulted in the 8 cases specified in Table 10, which are based on two different mass transfer correlations and four kinetic models. The selection was based on the lower deviation from experimental data shown in Fig. 4, Fig. 5, and Table S-2 of the Supporting Information. Additionally, and only for comparison purposes, the kinetic model proposed by Hikita et al.[38] was selected as exemplary case of a model considering second-order kinetics for the reaction of CO_2 with MEA and whose parameter estimation has been carried out using diluted aqueous MEA solutions.

Table 10. The selected cases for further analysis.

Model ID	Mass transfer correlation	Kinetic model
M1	Bravo et al.[88]	Hikita et al.[38]
M2	Hanley et al.[87]	Hikita et al.[38]
M3	Bravo et al.[88]	Aboudheir et al.[36]
M4	Hanley et al.[87]	Aboudheir et al.[36]
M5	Bravo et al.[88]	Luo et al.[73]
M6	Hanley et al.[87]	Luo et al.[73]
M7	Bravo et al.[88]	Luo et al.[6]-Model c
M8	Hanley et al.[87]	Luo et al.[6]-Model c

The liquid temperature, CO_2 partial pressure, and CO_2 mass fraction profiles based on EXP2 of pilot data are presented in Fig. 6. Models M3, M5, and M7 predict the three assessed profiles equally well, with the 5 other cases featuring larger deviation. This confirms that the mass transfer correlation of Bravo et al.[88] is more appropriate than the mass transfer correlation of Hanley et al.[87] Moreover, M3, M5, and M7 use the termolecular kinetic

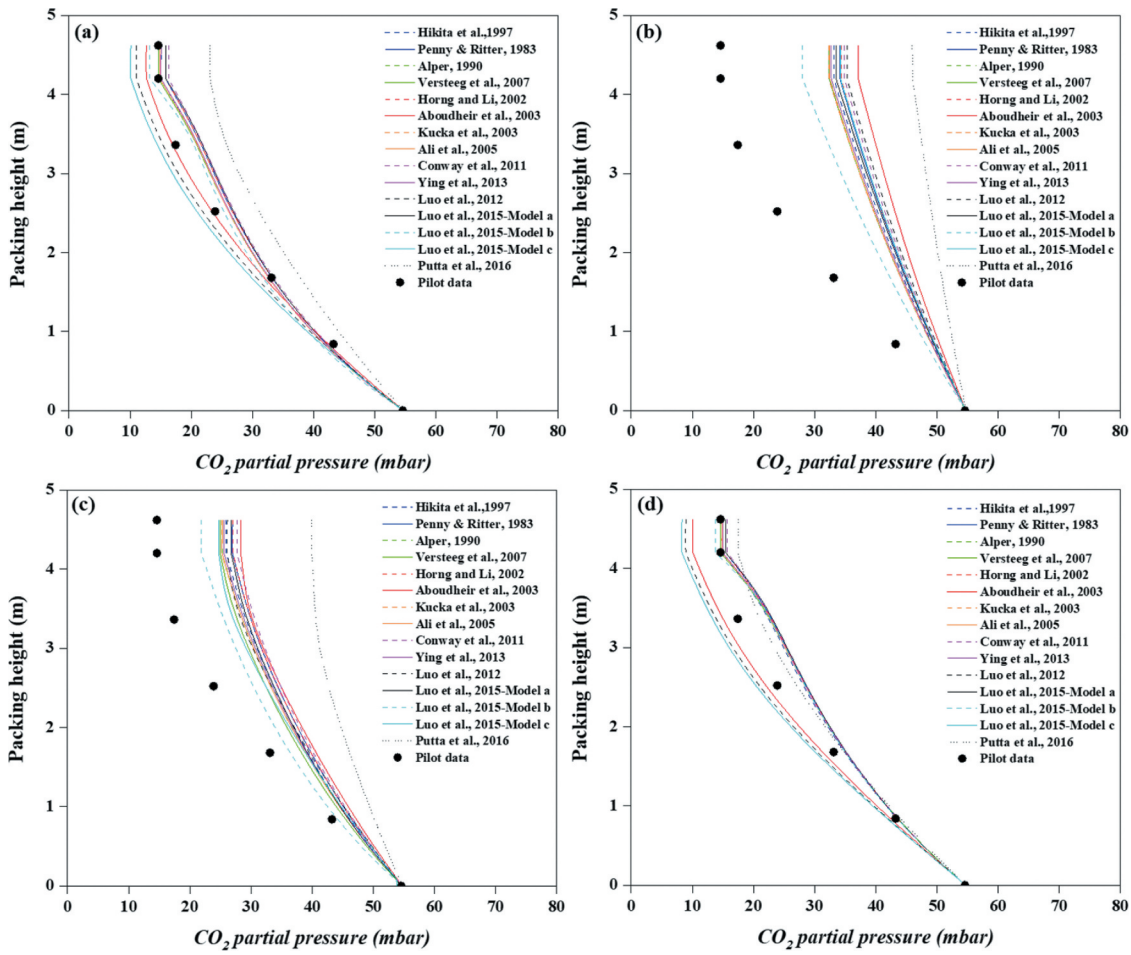

Figure 5. CO_2 partial pressure profiles predicted by models with different kinetic models and mass transfer correlations: (a) L. Bravo et al.,[88] (b) L. Bravo et al.,[89] (c) Billet and Schultes,[85] and (d) Hanley and Chen[87] based on EXP1 of pilot data.

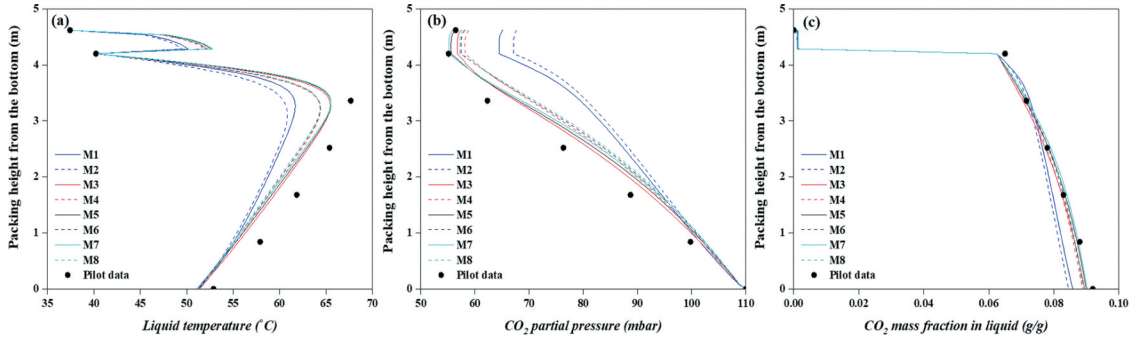

Figure 6. Prediction of (a) temperature profiles, (b) CO_2 partial pressure profiles, and (c) CO_2 mass fraction profiles by 8 selected rate-based models based on EXP2 of pilot data.

models of Aboudheir et al., [36] Luo et al.-2012, [73] and Luo et al.-2015-Model c, [6] respectively, while the consideration of a second-order kinetic model leads to predictions far from the experimental results. Further profiles in conditions of EXP3 and EXP6 for M1-8 are reported in figure S-7 of the Supporting Information.

The AARD% for EXP1 and EXP2 were ultimately calculated to select the best model (Table 11). Models M3 to M8 predict temperature profiles with deviation under 2% and 4% for EXP1 and EXP2, respectively. In term of CO_2 partial pressure (P_{CO_2}) AARD% was about 6% and 4% for EXP1 and EXP2, respectively. The significant deviation for the prediction of CO_2 partial pressure of EXP1 is likely due to the very low CO_2 partial pressure at the inlet flue gas of this experiment. This is consistent with previous reports in the case of low concentration of CO_2.[26,43] The combination Bravo et al.[88] and the kinetic model of Aboudheir et al.[36] (M3 as highlighted in Table 11) leads to the best result. This might come from (i) the experimental conditions used by Aboudheir et al., which are similar to the pilot plant tests, (ii) the utilization of the termolecular mechanism for the reaction of CO_2 with MEA that is able to reproduce a reaction rate order with respect to MEA concentration between 1 and 2, and (iii) the application of the penetration theory for the estimation of the kinetic parameters instead of the two-film theory with enhancement factor, which requires the assumption of pseudo-first-order kinetics. Indeed, as shown by Liu et al., [53] higher CO_2 partial pressure in the flue gas and NH_3 concentration and CO_2 loading in the liquid lead to significant depletion of the NH_3 concentration within the liquid film, from the bulk liquid to the vapor-liquid interphase, limiting the validity of the pseudo-first-order approach. In terms of CO_2 mass fraction in the liquid phase (w_{CO_2}) all models M3 to M8 show low deviations. The AARD% values based on EXP3 and EXP6 are reported in Table S-3 of the Supporting Information.

Table 11. The calculated AARD% of eight studied cases based on EXP1 and EXP2.

	EXP1			EXP2		
Model ID	Temperature (°C)	P_{CO_2} (mbar)	w_{CO_2} (g/g)	Temperature (°C)	P_{CO_2} (mbar)	w_{CO_2} (g/g)
M1	2.453	6.163	2.960	5.235	11.193	4.166
M2	2.685	9.076	2.201	5.771	12.749	4.750
M3	1.738	3.927	2.555	3.006	3.567	1.762
M4	1.453	9.995	1.732	3.728	5.831	1.827
M5	1.271	9.311	2.289	3.216	4.142	1.417
M6	1.130	13.723	1.761	3.854	5.988	1.706
M7	0.998	12.449	2.162	3.423	4.078	1.695
M8	0.961	15.671	1.880	3.974	6.249	1.854

Further comparisons (Table 12) included important process variables predicted by these 8 models for EXP1 and EXP2: temperatures of outlet gas and liquid, CO_2 mass fraction in outlet liquid (w_{CO_2}), partial pressure of CO_2 in outlet gas (P_{CO_2}), CO_2 rich loading (α_{CO_2}), and CO_2 capture efficiency. The highlighted values in Table 12 identify the cases with lowest error. M3 and M7 features the lowest ARD% based on EXP1 and EXP2, respectively. Considering the experimental conditions, we can conclude that M3 is better for CO_2 capture process from natural gas power plant-like flue gases, while M7 is better for coal-fired power plant-like flue gases. The predicted values based on EXP1, EXP2, EXP3, and EXP6 of pilot data are reported in Tables S-4 and S-5 of the Supporting Information.

Overall, when considering the average of both ARD% and AARD% from experimental data EXP1, EXP2, EXP3, and EXP6 (with equal weight for all cases) M3 is the best performing model, as shown in Table 13. Such results have been confirmed from the ANOVA statistical analysis that, for the sake of readability, have been included in the Supporting Information (Figure S-8).

The effect of different holdup correlations was studied based on the selected model (M3). The three available holdup correlations in Aspen Plus rate-based framework, which include Bravo et al., [89] Stichlmair et al., [95] and Billet and Schultes[85] were used for the holdup calculation. It should be noted that the holdup

Table 12. The value of ARD % of different process variables, predicted by eight studied cases with based on EXP1 and EXP2.

	EXP1						EXP2					
Model ID	Temperature (°C), (Liquid outlet)	Temperature (°C), (Gas outlet)	w_{CO_2} (g/g), (Liquid outlet)	P_{CO_2} (mbar), (Gas outlet)	α_{CO_2} (mol_{CO2}/mol_{MEA})	CO_2 captured (%)	Temperature (°C), (Liquid outlet)	Temperature (°C), (Gas outlet)	w_{CO_2} (g/g), (Liquid outlet)	P_{CO_2} (mbar), (Gas outlet)	α_{CO_2} (mol_{CO2}/mol_{MEA})	CO_2 captured (%)
M1	2.430	3.719	2.596	11.372	2.620	3.412	0.072	4.857	6.722	16.948	6.895	17.747
M2	2.210	3.815	2.439	9.848	2.497	2.997	0.227	3.257	8.096	21.661	8.323	22.129
M3	2.035	3.403	0.983	6.294	0.938	2.116	0.200	8.663	2.726	3.173	2.785	5.110
M4	2.113	4.446	0.774	25.376	0.868	8.063	0.341	7.776	3.465	5.685	3.562	7.489
M5	2.302	4.072	0.119	18.355	0.211	5.890	0.423	9.326	2.142	1.151	2.194	3.293
M6	2.252	4.963	1.568	34.031	1.693	10.772	0.456	8.186	3.095	4.406	3.187	6.335
M7	2.450	4.448	0.741	25.174	0.860	8.024	0.588	9.633	1.913	0.353	1.966	2.593
M8	2.306	5.249	1.989	38.615	2.129	12.207	0.539	8.345	2.979	4.000	3.071	5.980

Table 13. The average of deviations of models from all four experiments. The best performing model is highlighted.

Model ID	Average of ARD%	Average of AARD%
M1	6.450	5.571
M2	7.021	5.583
M3	5.499	3.965
M4	6.694	4.842
M5	5.990	4.012
M6	9.849	5.352
M7	28.253	13.642
M8	6.030	5.369

correlation by Bravo et al.[89] had been fixed so far. When comparing the process variables, no remarkable difference between the implemented correlations are found. For both EXP1 and EXP2, the difference of obtained ARD% between different models are in the order of 10^{-3} which can be neglected.

Analysis of the best performing model

The overall performance assessment of the rate-based model of the CO_2 absorber selected in this work, M3, was carried out. Figure 7 depicts the parity plots of model predictions for the CO_2 rich loading (liquid phase) and CO_2 capture efficiency (gas phase) based on all 47 experiments of Notz et al. pilot data.[55] As is shown in Fig. 7, M3 is able to predict all 47 experiment within an error range of ±7% (indicated by dashed lines).

Additionally, we have compared in Table 14 the key features of our selected rate-based model M3 with other rate-based models proposed in literature built upon Notz et al. experimental data.

First of all, the model proposed in this work has been tested using all experimental data. While the models presented by Aspen Technology, [50] Kale et al., [56] and Li et al., [52] might perform better for selected experiments, their performance is uncertain for the pilot tests not considered in the model development. Therefore, we believe our model is overall more reliable compared to those available in the open literature. As a matter of fact, only Luo and Wang[47] validated the model using a significant amount of available experiments, i.e., 22 out of 47 reported by Notz et al.[55] Aiming at comparing the performance of the rate-based model proposed in this work and that of Luo and Wang, Table 15 compares the AARD% obtained by means of each model for the prediction of the experimental values of the CO_2 capture efficiency and of the

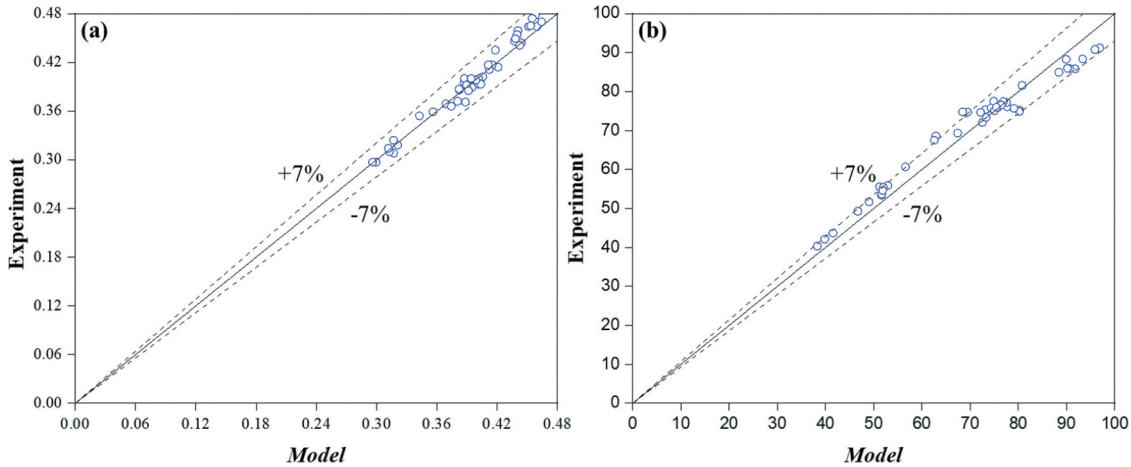

Figure 7. Parity plots of rate-based model, M3, predictions and the experimental data reported by Notz et al..[55] (a) Rich CO_2 loading ($mol_{CO2}.mol^{-1}_{MEA}$) and (b) CO_2 captured efficiency (%).

Table 14. Main features of different CO_2 capture rate-based models available in literature implemented in Aspen Plus for the CO_2 absorber of post-combustion CO_2 capture processes using aqueous MEA as solvent.

	Aspen Technology[50]	Kale et al.[56]	Li et al.[52]	Luo and Wang[47]	This work
Variables	Characteristics of models				
Mass transfer correlation	Bravo et al.[88]	Rocha et al.[97]	Bravo et al.[88]	Billet and schultes[85]	Bravo et al.[88]
Kinetic parameters	Hikita et al.[38]	Hikita et al[38]	Hikita et al[38]	Hikita et al[38]	Aboudheir et al.[36]
Thermodynamic model	e-NRTL	e-NRTL	e-NRTL	e-NRTL	e-NRTL
Vapor EOS	RK	SRK	RK	PC-SAFT	SRK
Axial discretization (m/segment)	0.233	0.168	0.21	0.105	0.084
Type of film discretization	Geometric	Not specified	Geometric	Not specified	Geometric
NDP	5	1	5	20	6
FDR	5	1	5	Not specified	1.5
Number of experiments used for validation of model	1	2	6	22	47(All experiments)
Column heat loss	NO*	NO	NO	Not specified	YES

*NO: not considered

Table 15. The AARD% of the rate-based model proposed in this work and by Luo and Wang[47] with respect to the experimental results reported for the pilot tests of Notz et al.

Variable	Luo and Wang[47] (22 experiments)	This work (same 22 experiments used for validations by Luo and Wang)	This work (all 47 experiments)
CO_2 capture level (%)	1.78	3.51	3.94
Rich CO_2 loading (mol_{CO2}/mol_{MEA})	1.54	2.00	1.86

rich CO_2 loading reported in the same 22 experiments from Notz et al. used by Luo and Wang for the validation of their model. Additionally, Table 15 provides the AARD% obtained using the model proposed in this work for all 47 experiments of Notz et al.

The AARD% obtained by means of the model of Luo and Wang[47] are smaller than the AARD% resulting from applying the model proposed in this work for the 22 experiments of Notz et al. used by Luo and Wang. Nevertheless, the AARD% obtained by the model proposed in this work is lower than 4% in all cases, even when reproducing all 47 experiments of Notz et al. In addition, Fig. 8 compares the profiles along the column predicted by these two models of the temperature and the CO_2 mass fraction in the liquid phase for three exemplary experiments of Notz et al. It is worth noting that while the water-wash section has been included in the validation of our model, Luo and Wang[47] only focused on the CO_2 capture section of the absorber. Although both models are able to capture the trends and reproduce the profiles along the column, the model of Luo and Wang[47] appears to be less accurate despite the larger number of liquid film discretization points (20 instead of having 6 as in our case).

It is worth noting that only our rate-based model considers the experimental heat losses reported in literature (Luo and Wang[47] do not specify if the heat loss values were considered in their model validation). However, it is expected that heat loss is minimized in test rigs by means of proper insulation of the process units and piping, so that neither the model selection nor the performance of the model is affected if experimental heat loss values are neglected. The performance of our model with and without considering the experimental heat loss values is provided in the Supporting Information: Figure S-9 and Table S-7.

Considering all the features aforementioned, the rate-based model proposed in this work can be regarded as a significant advancement in the state of the art for the simulation of the CO_2 absorber (and water-wash column) of post-combustion CO_2 capture processes using aqueous MEA solutions, thus making it suitable for full process simulation and optimization.

Conclusion

Rate-based modeling of the CO_2 capture process using MEA solvent was performed using Aspen Plus, the e-NRTL method for liquid phase properties, and the SRK equation of state for vapor phase properties. The results of the 47 pilot plant experiments reported by Notz et al.[55] were used to calibrate the model and assess its accuracy. Aiming at an accurate, yet computationally efficient rigorous rate-based model, the axial discretization of the column and the liquid film discretization were analyzed for the absorber column. The application of different combinations of reaction kinetics and mass transfer and interfacial area correlations available in the literature showed that a proper selection is of paramount importance for the accuracy of the rate-based model. Those kinetic models obtained at typical operating conditions of the CO_2 absorber of the CO_2 capture plant that use the termolecular mechanism to describe the reaction between CO_2 and MEA in the liquid phase led to the most accurate predictions of the experimental results. Compared to the rate-based models available in the literature for the same unit operation and solvent

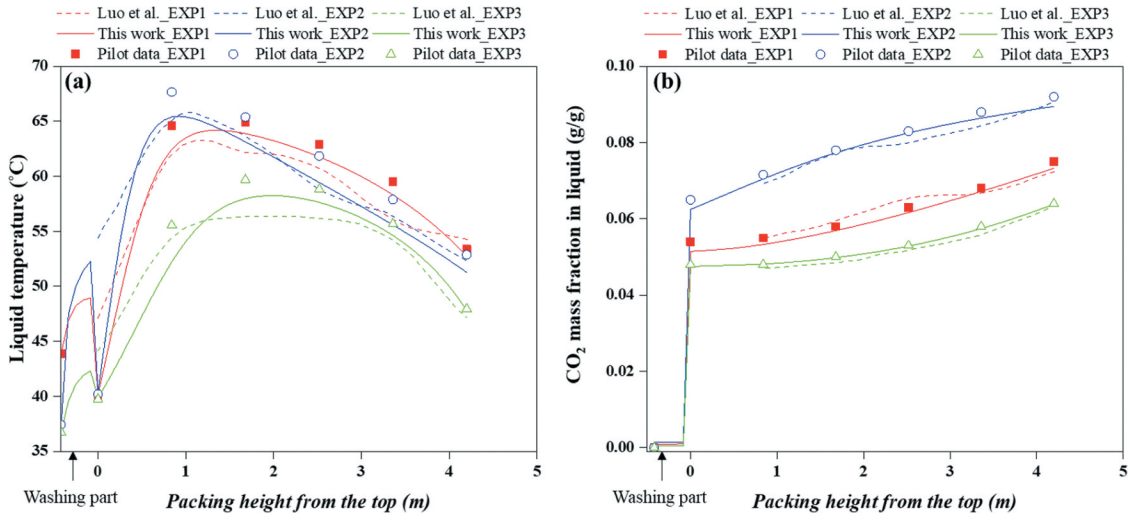

Figure 8. Temperature (a) and CO_2 mass fraction (b) of the liquid phase along the pilot plant CO_2 absorber for three exemplary experiments reported by Notz et al., EXP1, EXP2, and EXP3 of pilot data,[55] together with the profiles predicted by rate-based model proposed in this work and the model obtained by Luo and Wang.[47].

system, the rate-based model developed in this work can be considered to be: (i) more reliable, since it has been validated using a greater number of pilot plant experiments, (ii) more accurate, not only when predicting the specifications of the outlet streams but also the experimental profiles along the column, and (iii) computationally more efficient since it does not require a complex discretization of the liquid film. Thus, summarizing, its reliability, accuracy, and computational efficiency make the rate-based model proposed an advanced tool for the simulation and optimization of post-combustion CO_2 capture processes using an aqueous MEA solution as absorbent.

Acknowledgements

This research did not receive any specific grant from funding agencies in the public commercial, or not-for-profit sector.

ORCID

José-Francisco Pérez-Calvo http://orcid.org/0000-0003-2716-8367

Conflicts of interest statement

The authors whose name are listed immediately below certify that they have NO affiliations with or involvement in any organization or entity with any financial interest or non-financial interest in the subject matter or materials discuss in this manuscript.

Novelty statement

This research study presents a rigorous rate-based model for the absorption column in post- combustion CO2 capture processes. We considered most of the important parameters of a rate-based model (e.g., kinetic model, mass transfer correlation, liquid holdup, etc.) through the current modeling. Compared to the rate-based models available in the literature for the same unit operation and solvent system, the rate-based model developed in this work can be considered to be: (i) more reliable, since it has been validated using a greater number of pilot plant experiments, (ii) more accurate, not only when predicting the specifications of the outlet streams but also the experimental profiles along the column, and (iii) computationally more efficient since it considers simpler column discretization. Therefore, its reliability, accuracy, and computational efficiency makes the rate-based model proposed in this work an advanced tool for the simulation and optimization of post-combustion CO2 capture processes using an aqueous MEA solution as absorbent. In addition, we provide not only guidelines to implement a framework in Aspen Plus to simulate CO2 capture using aqueous MEA but also a comprehensive procedure to implement rate-based models for new solvents in reactive absorption process simulation. In this research work, the complications of CO2 capture and provide a versatile model for the simulation and optimization of CO2 capture processes.

Suplementary material

Supplemental data for this article can be accessed on Publsihers's website.

References

[1] Zhang, X.; Song, P.; Jiang, L. Performance Evaluation of an Integrated Redesigned Coal Fired Power Plant with CO2 Capture by Calcium Looping Process. Applied Thermal Engineering. 2020, 170, 115027. DOI: 10.1016/j.applthermaleng.2020.115027.

[2] Salvinder, K. M. S.; Zabiri, H.; Taqvi, S. A.; Ramasamy, M.; Isa, F.; Rozali, N. E. M.; Suleman, H.;

Maulud, A.; Shariff, A. M. An Overview on Control Strategies for CO2 Capture Using Absorption/stripping System. *Chemical Engineering Research and Design*. 2019, 147, 319–337. DOI: 10.1016/j.cherd.2019.04.034.

[3] Marx-Schubach, T.; Schmitz, G. Modeling and Simulation of the Start-up Process of Coal Fired Power Plants with Post-combustion CO2 Capture. *Int. J. Greenhouse Gas Con.* 2019, 87, 44–57. DOI: 10.1016/j.ijggc.2019.05.003.

[4] Arnaiz del Pozo, C.; Cloete, S.; Cloete, J.; Jiménez Álvaro, Á.; Amini, S. The Potential of Chemical Looping Combustion Using the Gas Switching Concept to Eliminate the Energy Penalty of CO2 Capture. International Journal of Greenhouse Gas Control, 2019, 83, 265–281. DOI: 10.1016/j.ijggc.2019.01.018.

[5] Luis, P.;. Use of Monoethanolamine (MEA) for CO2 Capture in a Global Scenario: Consequences and Alternatives. *Desalination*. 2016, 380, 93–99. DOI: 10.1016/j.desal.2015.08.004.

[6] Luo, X.; Hartono, A.; Hussain, S.; F. Svendsen, H. Mass Transfer and kinetics of carbon dioxide absorption into loaded aqueous monoethanolamine solutions. Chemical Engineering Science, 2015, 123, 57–69. DOI: 10.1016/j.ces.2014.10.013.

[7] Boot-Handford, M. E.; Abanades, J. C.; Anthony, E. J.; Blunt, M. J.; Brandani, S.; Mac Dowell, N.; Fernández, J. R.; Ferrari, M. C.; Gross, R.; Hallett, J. P.; Haszeldine, R. S.; Heptonstall, P.; Lyngfelt, A.; Makuch, Z.; Mangano, E.; Porter, R. T. J.; Pourkashanian, M.; Rochelle, G. T.; Shah, N.; Yao, J. G.; Fennell, P. S. Carbon Capture and Storage Update. Energy and Environmental Science. 2014, 7, 130–189. DOI: 10.1039/C3EE42350F.

[8] Bui, M.; Adjiman, C. S.; Bardow, A.; Anthony, E. J.; Boston, A.; Brown, S.; Fennell, P. S.; Fuss, S.; Galindo, A.; Hackett, L. A.; Hallett, J. P.; Herzog, H. J.; Jackson, G.; Kemper, J.; Krevor, S.; Maitland, G. C.; Matuszewski, M.; Metcalfe, I. S.; Petit, C.; Puxty, G.; Reimer, J.; Reiner, D. M.; Rubin, E. S.; Scott, S. A.; Shah, N.; Smit, B.; Trusler, J. P. M.; Webley, P.; Wilcox, J.; Mac Dowell, N. Carbon Capture and storage (CCS): the way forward. Energy & Environmental Science. 2018, 11(5),1062–1176. doi:10.1039/C7EE02342A

[9] Iijima, M.; Nagayasu, T.; Kamijyo, T.; Nakatani, S. MHI's Energy Efficient Flue Gas CO2 Capture Technology and Large Scale CCS Demonstration Test at Coal-fired Power Plants in USA. *Mitsubishi Heavy Ind. Tech. Rev.* 2011, 48, 26–32.

[10] Singh, A.; Stéphenne, K. Shell Cansolv CO2 Capture Technology: Achievement from First Commercial Plant. *Energy Procedia*. 2014, 63, 1678–1685. DOI: 10.1016/j.egypro.2014.11.177.

[11] Knudsen, J. N.; Bade, O. M.; Askestad, I.; Gorset, O.; Mejdell, T.Pilot Plant Demonstration of CO2 Capture from Cement Plant with Advanced Amine Technology. *Energy Procedia*. 2014, 63, 6464–6475. DOI: 10.1016/j.egypro.2014.11.682.

[12] Wang, S.; Su, Z.; Lu, X. Energy-consumption Analysis of Carbon-based Material for CO2 Capture Process. Fluid Phase Equilibria. 2020, 510, 112504. doi:10.1016/j.fluid.2020.112504

[13] Nocito, F.; Dibenedetto, A. Atmospheric CO2 Mitigation Technologies: Carbon Capture Utilization and Storage. *Curr. Opin. Green Sustain. Chem.* 2020, 21, 34–43. DOI: 10.1016/j.cogsc.2019.10.002.

[14] Kalatjari, H. R.; Haghtalab, A.; Nasr, M. R. J.; Heydarinasab, A. Experimental, simulation and thermodynamic modeling of an acid gas removal pilot plant for CO2 capturing by mono-ethanol amine solution. Journal of Natural Gas Science and Engineering 2019, 72, 103001. DOI: 10.1016/j.jngse.2019.103001.

[15] Razi, N.; Svendsen, H. F.; Bolland, O. Cost and Energy Sensitivity Analysis of Absorber Design in CO2 Capture with MEA. *Int. J. Greenhouse Gas Con.* 2013, 19, 331–339. DOI: 10.1016/j.ijggc.2013.09.008.

[16] Sohaib, Q.; Muhammad, A.; Younas, M.; Rezakazemi, M. Modelling pre-combustion CO2 capture with tubular membrane contactor using ionic liquids at elevated temperatures. Separation and Purification Technology 2020, 241, 116677. doi:10.1016/j.seppur.2020.116677

[17] Afkhamipour, M.; Mofarahi, M. Comparison of Rate-based and Equilibrium-stage Models of a Packed Column for Post-combustion CO2 Capture Using 2-amino-2-methyl-1-propanol (AMP) Solution. *Int. J. Greenhouse Gas Con.* 2013, 15, 186–199. DOI: 10.1016/j.ijggc.2013.02.022.

[18] Mores, P.; Scenna, N.; Mussati, S. A Rate Based Model of A Packed Column for CO2 Absorption Using Aqueous Monoethanolamine Solution. *Int. J. Greenhouse Gas Con.* 2012, 6, 21–36. DOI: 10.1016/j.ijggc.2011.10.012.

[19] Stewart, W. E.;. Multicomponent Mass Transfer. By Ross Taylor and R. Krishna, Wiley, New York, 1993, 579 pp. *AIChE J.* 1995, 41(1), 202–203. DOI: 10.1002/aic.690410124.

[20] Lawal, A.; Wang, M.; Stephenson, P.; Yeung, H. Dynamic Modelling of CO2 Absorption for Post Combustion Capture in Coal-fired Power Plants. *Fuel*. 2009, 88(12), 2455–2462.

[21] Higler, A.; Taylor, R.; Krishna, R. Modeling of a Reactive Separation Process Using a Nonequilibrium Stage Model. *Comput. Chem. Eng.* 1998, 22, S111–S118. DOI: 10.1016/S0098-1354(98)00044-1.

[22] Aronu, U. E.; Gondal, S.; Hessen, E. T.; Haug-Warberg, T.; Hartono, A.; Hoff, K. A.; Svendsen, H. F. Solubility of CO2 in 15, 30, 45 and 60 Mass% MEA from 40 to 120°C and Model Representation Using the Extended UNIQUAC Framework. Chemical Engineering Science 2011, 66(24),6393–6406. doi:10.1016/j.ces.2011.08.042

[23] Harris, F.; Kurnia, K. A.; Mutalib, M. I. A.; Thanapalan, M. Solubilities of Carbon Dioxide and Densities of Aqueous Sodium Glycinate Solutions before and after CO2 Absorption. *J. Chem. Eng. Data*. 2009, 54(1), 144–147.

[24] MD, H.;, A Predictive Thermodynamic Model for an Aqueous Blend of Potassium Carbonate, Piperazine, and Monoethanolamine for Carbon Dioxide Capture from Flue Gas [dissertation]. 2008, Austin: University of Texas at Austin.

[25] Tong, D.; Trusler, J. P. M.; Maitland, G. C.; Gibbins, J.; Fennell, P. S. Solubility of Carbon Dioxide in Aqueous Solution of Monoethanolamine or 2-amino-2-methyl-1-propanol: Experimental Measurements and Modelling. *Int. J. Greenhouse Gas Con.* 2012, 6, 37–47. DOI: 10.1016/j.ijggc.2011.11.005.

[26] Wagner, M.; von Harbou, I.; Kim, J.; Ermatchkova, I.; Maurer, G.; Hasse, H. Solubility of Carbon Dioxide in Aqueous Solutions of Monoethanolamine in the Low and High Gas Loading Regions. J.Chem. Eng. Data. 2013, 58(4),883–895. doi: 10.1021/je301030z

[27] Pitzer, K. S.;. Thermodynamics of Electrolytes. I. Theoretical Basis and General Equations. *J. Phys. Chem.* 1973, 77(2), 268–277. DOI: 10.1021/j100621a026.

[28] Pitzer, K. S.;. Thermodynamics of Electrolytes. V. Effects of Higher-order Electrostatic Terms. *J. Solution Chem.* 1975, 4(3), 249–265. DOI: 10.1007/BF00646562.

[29] Chen, -C.-C.; Evans, L. B. A Local Composition Model for the Excess Gibbs Energy of Aqueous Electrolyte Systems. *AIChE J.* 1986, 32(3), 444–454. DOI: 10.1002/aic.690320311.

[30] Langè, S.; Pellegrini, L. A.; Moioli, S.; Picutti, B.; Vergani, P. Influence of Gas Impurities on Thermodynamics of Amine Solutions. 2. Mercaptans. *Ind. Eng. Chem. Res.* 2013, 52(5), 2025–2031.

[31] Pellegrini, L. A.; Moioli, S.; Gamba, S.; Ceragioli, P. Prediction of vapor–liquid equilibrium for reservoir mixtures with cubic equations of state: Binary interaction parameters for acidic gases. Fluid Phase Equilibria. 2012, 326, 45–49. DOI: 10.1016/j.fluid.2012.03.030.

[32] Austgen, D. M.; Rochelle, G. T.; Peng, X.; Chen, C. C. Model of Vapor-liquid Equilibria for Aqueous Acid Gas-alkanolamine Systems Using the electrolyte-NRTL Equation. Ind. Eng. Chem. Res. 1989, 28(7),1060–1073. doi:10.1021/ie00091a028

[33] Faramarzi, L.; Kontogeorgis, G. M.; Thomsen, K.; Stenby, E. H. Extended UNIQUAC Model for Thermodynamic Modeling of CO2 Absorption in Aqueous Alkanolamine Solutions. Fluid Phase Equilibria. 2009, 282(2),121–132. doi:10.1016/j.fluid.2009.05.002

[34] Haghtalab, A.; Dehghani Tafti, M. Electrolyte UNIQUAC–NRF Model to Study the Solubility of Acid Gases in Alkanolamines. *Ind. Eng. Chem. Res.* 2007, 46(18), 6053–6060. DOI: 10.1021/ie070259r.

[35] Razi, N.; Svendsen, H. F.; Bolland, O. Validation of Mass Transfer Correlations for CO2 Absorption with MEA Using Pilot Data. *Int. J. Greenhouse Gas Con.* 2013, 19, 478–491. DOI: 10.1016/j.ijggc.2013.10.006.

[36] Aboudheir, A.; Tontiwachwuthikul, P.; Chakma, A.; Idem, R. Kinetics of the Reactive Absorption of Carbon Dioxide in High CO2-loaded, Concentrated Aqueous Monoethanolamine Solutions. Chemical Engineering Science 2003, 58(23–24), 5195–5210. doi:10.1016/j.ces.2003.08.014

[37] Alper, E.; Reaction Mechanism and Kinetics of Aqueous Solutions of 2-amino-2-methyl-1-propanol and Carbon Dioxide. *Ind. Eng. Chem. Res.* 1990, 29(8), 1725–1728. DOI: 10.1021/ie00104a023.

[38] Hikita, H.; Asai, S.; Ishikawa, H.; Honda, M. The Kinetics of Reactions of Carbon Dioxide with Monoethanolamine, Diethanolamine and Triethanolamine by a Rapid Mixing Method. *Chem. Eng. J.* 1977, 13(1), 7–12.

[39] Horng, S.-Y.; Li, M.-H. Kinetics of Absorption of Carbon Dioxide into Aqueous Solutions of Monoethanolamine + Triethanolamine. *Ind. Eng. Chem. Res.* 2002, 41(2), 257–266. DOI: 10.1021/ie010671l.

[40] Jamal, A.; Meisen, A.; Jim Lim, C. Kinetics of Carbon Dioxide Absorption and Desorption in Aqueous Alkanolamine Solutions Using a Novel Hemispherical contactor—II: Experimental Results and Parameter Estimation. *Chem. Eng. Sci.* 2006, 61(19), 6590–6603. DOI: 10.1016/j.ces.2006.04.047.

[41] Kucka, L.; Richter, J.; Kenig, E. Y.; Górak, A. Determination of Gas–liquid Reaction Kinetics with a Stirred Cell Reactor. *Sep. Purif. Technol.* 2003, 31(2), 163–175.

[42] Faramarzi, L.; Kontogeorgis, G. M.; Michelsen, M. L.; Thomsen, K.; Stenby, E. H. Absorber Model for CO2 Capture by Monoethanolamine. *Ind. Eng. Chem. Res.* 2010, 49(8), 3751–3759.

[43] Moioli, S.; Pellegrini, L. A.; Picutti, B.; Vergani, P. Improved Rate-Based Modeling of H2S and CO2 Removal by Methyldiethanolamine Scrubbing. *Ind. Eng. Chem. Res.* 2013, 52(5), 2056–2065.

[44] Kenig, E. Y.; Gorak, A. Modelling of Multicomponent Mass Transfer in Separation of Fluid Systems: Basics and Peculiarities. *Chem. Process. Eng-Inz.* 1999, 20(3), 327–349.

[45] Taylor, R.; Krishna, R. *Multicomponent Mass Transfer*; New York: Wiley, 1993.

[46] Lewis, W. K.; Whitman, W. G. Principles of Gas Absorption. *Ind. Eng. Chem.* 1924, 16(12), 1215–1220. DOI: 10.1021/ie50180a002.

[47] Luo, X.; Wang, M. Improving Prediction Accuracy of a Rate-Based Model of an MEA-Based Carbon Capture Process for Large-Scale Commercial Deployment. *Engineering*. 2017, 3(2), 232–243. DOI: 10.1016/J.ENG.2017.02.001.

[48] von Harbou, I.; Imle, M.; Hasse, H. Modeling and Simulation of Reactive Absorption of CO2 with MEA: Results for Four Different Packings on Two Different Scales. *Chem. Eng. Sci.* 2014, 105, 179–190. DOI: 10.1016/j.ces.2013.11.005.

[49] Tobiesen, F. A.; Svendsen, H. F.; Juliussen, O. Experimental Validation of a Rigorous Absorber Model for CO2 Postcombustion Capture. *AIChE J.* 2007, 53(4), 846–865. DOI: 10.1002/aic.11133.

[50] Aspen Plus.;. Rate-based Model of the CO2 Capture Process by MEA Using Aspen Plus. Aspen Technology. 2012. Burlington (USA).

[51] Gáspár, J.; Cormoş, A.-M. Dynamic Modeling and Validation of Absorber and Desorber Columns for Post-combustion CO2 Capture. *Comput. Chem. Eng.* 2011, 35(10), 2044–2052. DOI: 10.1016/j.compchemeng.2010.10.001.

[52] Li, B.-H.; Zhang, N.; Smith, R. Simulation and Analysis of CO2 Capture Process with Aqueous Monoethanolamine Solution. *Appl. Energy*. 2016, 161, 707–717. DOI: 10.1016/j.apenergy.2015.07.010.

[53] Liu, J.; Gao, H-C.; Peng, C-C; Wong, D. S-H.; Jang, S-S.; Shen, J-F. Aspen Plus Rate-based Modeling for Reconciling Laboratory Scale and Pilot Scale CO2 Absorption Using Aqueous Ammonia. Int. J. Greenhouse Gas Con. 2015, 34, 117–128. DOI: 10.1016/j.ijggc.2015.01.009.

[54] Zhang, Y.; Chen, H.; Chen, C.; Plaza, J. M.; Dugas, R.; Rochelle, G. T. Rate-Based Process Modeling Study of

CO2 Capture with Aqueous Monoethanolamine Solution. Ind. Eng. Chem. Res. 2009, 48(20),9233–9246. doi:10.1021/ie900068k

[55] Notz, R.; Mangalapally, H. P.; Hasse, H. Post Combustion CO2 Capture by Reactive Absorption: Pilot Plant Description and Results of Systematic Studies with MEA. *Int. J. Greenhouse Gas Con.* 2012, 6, 84–112. DOI: 10.1016/j.ijggc.2011.11.004.

[56] Kale, C.; Górak, A.; Schoenmakers, H. Modelling of the Reactive Absorption of CO2 Using Mono-ethanolamine. *Int. J. Greenhouse Gas Con.* 2013, 17, 294–308. DOI: 10.1016/j.ijggc.2013.05.019.

[57] Peng, J.; Lextrait, S.; Edgar, T. F.; Eldridge, R. B. A Comparison of Steady-State Equilibrium and Rate-Based Models for Packed Reactive Distillation Columns. Ind. Eng. Chem. Res. 2002, 41(11),2735–2744. doi:10.1021/ie010969b

[58] Amirkhosrow, M.; Nemati Lay, E. Simulation Model Evaluation of Desorber Column in CO2 Capture Process by MEA Scrubbing: A Rigorous Rate-based Model for Kinetic Model and Mass Transfer Correlations Analysis. *Fuel Process. Technol.* 2020, 203, 106390. DOI: 10.1016/j.fuproc.2020.106390.

[59] Moioli, S.; Pellegrini, L. A. Improved Rate-based Modeling of the Process of CO2 Capture with PZ Solution. *Chemical Engineering Research and Design*. 2015, 93, 611–620. DOI: 10.1016/j.cherd.2014.03.022.

[60] Soave, G.;. Equilibrium Constants from a Modified Redlich-Kwong Equation of State. *Chem. Eng. Sci.* 1972, 27(6), 1197–1203. DOI: 10.1016/0009-2509(72)80096-4.

[61] Liu, Y.; Zhang, L.; Watanasiri, S. Representing Vapor–Liquid Equilibrium for an Aqueous MEA–CO2 System Using the Electrolyte Nonrandom-Two-Liquid Model. *Ind. Eng. Chem. Res.* 1999, 38(5), 2080–2090. DOI: 10.1021/ie980600v.

[62] Edwards, T. J.; Maurer, G.; Newman, J.; Prausnitz, J. M. Vapor-liquid Equilibria in Multicomponent Aqueous Solutions of Volatile Weak Electrolytes. *AIChE J.* 1978, 24(6), 966–976.

[63] Kent, L. R.;. Better Data for Amine Treating. Hydrocarbon processing. 1976, 55(2),87–90.

[64] Caplow, M.;. Kinetics of Carbamate Formation and Breakdown. *J. Am. Chem. Soc.* 1968, 90(24), 6795–6803. DOI: 10.1021/ja01026a041.

[65] Danckwerts, P. V.;. The Reaction of CO2 with Ethanolamines. *Chem. Eng. Sci.* 1979, 34(4), 443–446. DOI: 10.1016/0009-2509(79)85087-3.

[66] Crooks, J. E.; Donnellan, J. P. Kinetics and Mechanism of the Reaction between Carbon Dioxide and Amines in Aqueous Solution. *J. Chem. Soc. Perkin Trans. I*. 1989, 2(4), 331–333. DOI: 10.1039/p29890000331.

[67] Kumar, P. S.; Hogendoorn, J. A.; Versteeg, G. F.; Feron, P. H. M. Kinetics of the Reaction of CO2 with Aqueous Potassium Salt of Taurine and Glycine. *AIChE J.* 2003, 49(1), 203–213.

[68] Penny, D. E.; Ritter, T. J. Kinetic Study of the Reaction between Carbon Dioxide and Primary Amines. *J. Chem. Soc., Faraday Trans. 1*. 1983, 79(9), 2103. DOI: 10.1039/f19837902103.

[69] Ali, S. H.;. Kinetics of the Reaction of Carbon Dioxide with Blends of Amines in Aqueous Media Using the Stopped-flow Technique. International Journal of Chemical Kinetics. 2005, 37(7),391–405. doi:10.1002/(ISSN)1097-4601

[70] Versteeg, G. F.; Van Dijck, L. A. J.; Van Swaaij, W. P. M. On the Kinetics Between CO2 and Alkanolamines Both in Aqueous and Non-Aqueous Solutions. An Overview. *Chem. Eng. Comm.* 1996, 144(1), 113–158. DOI: 10.1080/00986449608936450.

[71] Conway, W.; Wang, X.; Fernandes, D.; Burns, R.; Lawrance, G.; Puxty, G.; Maeder, M. Comprehensive Kinetic and Thermodynamic Study of the Reactions of CO2(Aq) and HCO3–With Monoethanolamine (MEA) in Aqueous Solution. *J. Phys. Chem. A*. 2011, 115(50), 14340–14349.

[72] Ying, J.; Eimer, D. A. Determination and Measurements of Mass Transfer Kinetics of CO2 in Concentrated Aqueous Monoethanolamine Solutions by a Stirred Cell. *Ind. Eng. Chem. Res.* 2013, 52(7), 2548–2559. DOI: 10.1021/ie303450u.

[73] Luo, X.; Hartono, A.; Svendsen, H. F. Comparative Kinetics of Carbon Dioxide Absorption in Unloaded Aqueous Monoethanolamine Solutions Using Wetted Wall and String of Discs Columns. *Chem. Eng. Sci.* 2012, 82, 31–43. DOI: 10.1016/j.ces.2012.07.001.

[74] Putta, K. R.; Pinto, D. D. D.; Svendsen, H. F.; Knuutila, H. K. CO2 absorption into loaded aqueous MEA solutions: Kinetics assessment using penetration theory. International Journal of Greenhouse Gas Control 2016, 53, 338–353. DOI: 10.1016/j.ijggc.2016.08.009.

[75] Brinkman, R.; Margaria, R.; Roughton, F. J. W.; Barcroft, J. The Kinetics of the Carbon Dioxide-carbonic Acid Reaction. Philosophical Transactions of the Royal Society of London. A, Containing Papers of a Mathematical or Physical Character 1933, 232(707–720), 65–97. doi:10.1098/rsta.1934.0003

[76] Himmelblau, D. M.; Babb, A. L. Kinetic Studies of Carbonation Reactions Using Radioactive Tracers. AIChE Journal. 1958, 4(2),143–152. doi:10.1002/(ISSN)1547-5905

[77] Kucka, L.; Kenig, E. Y.; Górak, A. Kinetics of the Gas–Liquid Reaction between Carbon Dioxide and Hydroxide Ions. *Ind. Eng. Chem. Res.* 2002, 41(24), 5952–5957. DOI: 10.1021/ie020452f.

[78] Puxty, G.; Maeder, M. 2 - the Fundamentals of Post-combustion Capture. In *Absorption-Based Post-combustion Capture of Carbon Dioxide*; Feron, P. H. M., Ed.; Woodhead Publishing, 2016; pp 13–33.

[79] Pinsent, B. R. W.; Pearson, L.; Roughton, F. J. W. The Kinetics of Combination of Carbon Dioxide with Ammonia. *Trans. Faraday Soc.* 1956, 52, 1594. DOI: 10.1039/tf9565201594.

[80] Razi, N.; Svendsen, H. F.; Bolland, O. Assessment of Mass Transfer Correlations in Rate-based Modeling of a Large-scale CO2 Capture with MEA. *Int. J. Greenhouse Gas Con.* 2014, 26, 93–108. DOI: 10.1016/j.ijggc.2014.04.019.

[81] Tönnies, I.; Mangalapally, H. P.; Hasse, H. Sensitivity Study for the Rate-based Simulation of the Reactive Absorption of CO2. *Energy Procedia*. 2011, 4, 533–540. DOI: 10.1016/j.egypro.2011.01.085.

[82] Kvamsdal, H. M.; Chikukwa, A.; Hillestad, M.; Zakeri, A.; Einbu, A. A Comparison of Different Parameter Correlation Models and the Validation of an MEA-based Absorber Model. Energy Procedia. 2011, 4, 1526–1533. DOI: 10.1016/j.egypro.2011.02.021.
[83] Razi, N.; Bolland, O.; Svendsen, H. Review of Design Correlations for CO2 Absorption into MEA Using Structured Packings. *Int. J. Greenhouse Gas Con.* 2012, 9, 193–219. DOI: 10.1016/j.ijggc.2012.03.003.
[84] Ataki, A.; Bart, H. J. Experimental and CFD Simulation Study for the Wetting of a Structured Packing Element with Liquids. *Chem. Eng. Technol.* 2006, 29(3), 336–347. DOI: 10.1002/ceat.200500302.
[85] Billet, R.; Schultes, M. Predicting Mass Transfer in Packed Columns. *Chem. Eng. Technol.* 1993, 16(1), 1–9. DOI: 10.1002/ceat.270160102.
[86] Brunazzi, E.; Paglianti, A. Liquid-Film Mass-Transfer Coefficient in a Column Equipped with Structured Packings. *Ind. Eng. Chem. Res.* 1997, 36(9), 3792–3799. DOI: 10.1021/ie970045h.
[87] Hanley, B.; Chen, -C.-C. New Mass-transfer Correlations for Packed Towers. *AIChE J.* 2012, 58(1), 132–152. DOI: 10.1002/aic.12574.
[88] Bravo, L.; Rocha, J. J. A.; Fair, J. R. Mass Transfer in Gauze Packing. Chemistry. 1985, 64, 91–95.
[89] Bravo, L.; Rocha, J. J. A.; Fair, J. R. Comprehensive Model for the Performance of Columns Containing Structured Packings. IChemE Symposium series. 1992, 128, A439.
[90] Albright, L. F.;. *Albright's Chemical Engineering Handbook*; CRC Press: Boca Raton [etc.], 2009.
[91] Billet, R.; Schultes, M. Modelling of Pressure Drop in Packed Columns. *Chem. Eng. Technol.* 1991, 14(2), 89–95. DOI: 10.1002/ceat.270140203.
[92] Bravo, J. L.; Rocha, J. A.; Fair, J. R. Pressure Drop in Structured Packings. *Hydrocar. Process.* 1986, 65, 3.
[93] Brunazzin, E.; Paglianti, A. Mechanistic Pressure Drop Model for Columns Containing Structured Packings. *AIChE J.* 1997, 43(2), 317–327. DOI: 10.1002/aic.690430205.
[94] Buchanan, J. E.;. Pressure Gradient and Liquid Holdup in Irrigated Packed Towers. *Indus. Eng. Chem. Fund.* 1969, 8(3), 502–511. DOI: 10.1021/i160031a022.
[95] Stichlmair, J.; Bravo, J. L.; Fair, J. R. General Model for Prediction of Pressure Drop and Capacity of Countercurrent Gas/liquid Packed Columns. *Gas Sep. Purif.* 1989, 3(1), 19–28. DOI: 10.1016/0950-4214(89)80016-7.
[96] Kvamsdal, H. M.; Rochelle, G. T. Effects of the Temperature Bulge in CO2 Absorption from Flue Gas by Aqueous Monoethanolamine. *Ind. Eng. Chem. Res.* 2008, 47(3), 867–875. DOI: 10.1021/ie061651s.
[97] Rocha, J. A.; Bravo, J. L.; Fair, J. R. Distillation Columns Containing Structured Packings: A Comprehensive Model for Their Performance. 2. Mass-Transfer Model. *Mass-Transfer Model. Industrial & Engineering Chemistry Research*. 1996, 35(5), 1660–1667. DOI: 10.1021/ie940406i.